A Novel and Scalable Spatio-Temporal Technique for Ocean Eddy Monitoring

James H. Faghmous[†], **Yashu Chamber**[†], **Shyam Boriah**[†], **Stefan Liess**[‡] and **Vipin Kumar**[†]
[†]Department of Computer Science and Engineering
[‡]Department of Soil, Water and Climate
University of Minnesota

Frode Vikebø
Institute of Marine Research
Bergen, Norway

Michel dos Santos Mesquita
Bjerknes Centre for Climate Research
Bergen, Norway

Abstract

Swirls of ocean currents known as ocean eddies are a crucial component of the ocean's dynamics. In addition to dominating the ocean's kinetic energy, eddies play a significant role in the transport of water, salt, heat, and nutrients. Therefore, understanding current and future eddy patterns is a central climate challenge to address future sustainability of marine ecosystems. The emergence of sea surface height observations from satellite radar altimeter has recently enabled researchers to track eddies at a global scale. The majority of studies that identify eddies from observational data employ highly parametrized connected component algorithms using expert filtered data, effectively making reproducibility and scalability challenging. In this paper, we frame the challenge of monitoring ocean eddies as an unsupervised learning problem. We present a novel change detection algorithm that automatically identifies and monitors eddies in sea surface height data based on heuristics derived from basic eddy properties. Our method is accurate, efficient, and scalable. To demonstrate its performance we analyze eddy activity in the Nordic Sea ($60 - 80^\circ$ N and 20° W $- 20^\circ$ E), an area that has received limited attention and has proven to be difficult to analyze using other methods.

1 Introduction

Rotating coherent structures of water, known as ocean eddies (hereby eddies) are considered the oceanic analog of storms in the atmosphere (Fu et al. 2010). Eddies dominate the ocean's kinetic energy and play a significant role in the transport of water, salt, heat and nutrients. Eddies have also been shown to impact marine ecosystems by raising the deep nutrient-rich water to the surface, which renews the nutrient supply to phytoplankton and subsequently leads to increased fish production (Denman and Gargett 1983). Furthermore, given eddies' demonstrated impact on near-surface chlorophyll concentration (Chelton et al. 2011), which is reflected in the green tint in ocean color (see Figure 1 top panel), eddies may impact hurricane tracks and landfall probabilities through changes in ocean color which in turn affect sea surface temperatures and large-scale circulation patterns (Gnanadesikan et al. 2010). Given such a critical impact on the oceans, understanding past and current eddy activity is crucial for forecasting future ocean dynamics and, subsequently, marine ecosystem sustainability.

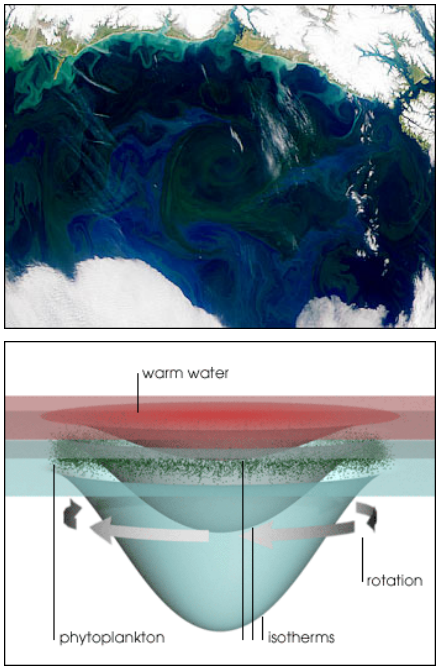

Figure 1: **Top:** An eddy off the coast of Alaska. Ocean eddies (green whirlpool in middle of figure) are rotating coherent structures of water. The rotational movement brings nutrients up towards the surface resulting in phytoplankton bloom and is reflected by the green color amidst blue water. **Bottom:** A cross section of a cyclonic eddy (in the Northern Hemisphere) that causes a decrease in SSH. Images courtesy of NASA.

Until recently, ocean eddies were tracked using sea surface temperatures (SST) and satellite images. Now, sea surface height (SSH) observations from satellite radar altimeters have emerged as a better suited alternative for studying eddy dynamics on a global scale. Eddies are generally classified as either cyclonic if they rotate counter-clockwise (in the Northern Hemisphere) or anti-cyclonic otherwise. Cyclonic eddies, like the one in Figure 1 (bottom panel), cause a decrease in SSH and elevations in subsurface density surfaces.

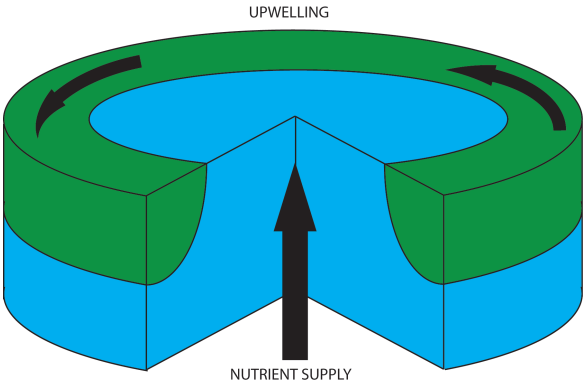

Figure 2: Density surfaces are lifted within a cyclonic eddy causing a decrease in SSH. The elevation of subsurface density surfaces replenishes the upper part of the ocean with nutrients needed for primary production.

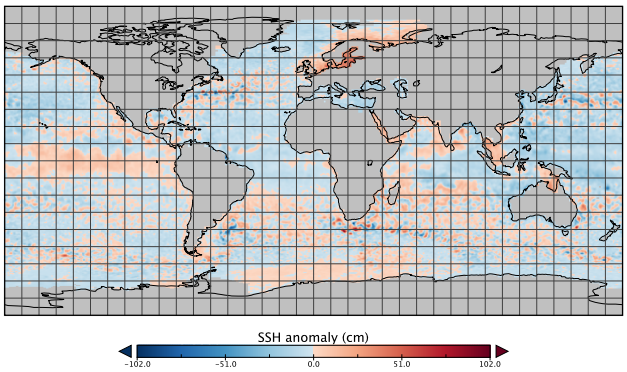

Figure 3: Global sea surface height (SSH) anomaly for the week of May 5 1993 from the AVISO dataset. Eddies can be observed globally as closed contoured negative (dark blue; for cyclonic) or positive (dark red; for anti-cyclonic) anomalies.

Anti-cyclonic eddies, such as the one depicted in Figure 2, cause an increase in SSH and depressions in subsurface density surfaces. These characteristics allow us to identify ocean eddies in SSH satellite data. In Figure 3, anti-cyclonic eddies can be seen in patches of positive (dark red) SSH anomalies, while cyclonic eddies are reflected in closed contoured negative (dark blue) SSH anomalies.

The majority of algorithms tracking eddies employ an image processing approach on satellite snapshots of SST or SSH. Image-based approaches often have computational and application-specific limitations (that we will discuss in more detail later). Furthermore, such algorithms are highly parameterized and rely on complex data-filtering schemes that make reproducibility challenging. We present an unsupervised algorithm that identifies and monitors eddies by analyzing changes in SSH anomaly time-series. This novel approach does not require any data pre-processing and proves to be more scalable and efficient than traditional tracking algorithms. To illustrate our algorithm's performance, we will focus on monitoring eddies in the Nordic Sea ($60 - 80^\circ$ N and 20° W $- 20^\circ$ E): a region that has received limited anecdotal attention (*e.g.* (Hansen, Kvaleberg, and Samuelsen 2010)). Another advantage of using this region for evaluation is that it does not suffer from the potential of confusing Rossby waves (large-scale ocean variability known as the "internal weather of the sea") with ocean eddies, a problem that until recently was very common at lower latitudes (Chelton et al. 2011).

Designing intelligent, reproducible and scalable algorithms is crucial for high impact research in oceanography and related fields, and this work is a first step in that direction. In the next section, we will briefly review existing eddy tracking algorithms. In the following section, we will introduce our change detection algorithm, *persistent delta* (PDELTA), which leverages the unique spatio-temporal characteristic of ocean eddies. After that, we will present our results and compare them to the eddies identified by Chelton, Schlax, and Samelson (2011) (CH11 thereafter). We will also compare PDELTA's scalability to that of a connected component algorithm that is similar to the one used by CH11. We conclude the paper with a discussion of the study's contributions and future research directions.

2 Previous Work

Techniques for automatic identification and tracking of ocean eddies are largely based on image processing algorithms. Such approaches rely primarily on proxy variables such as ocean color or SST. The main challenge when using such proxies to track eddies is that they are influenced by a variety of factors, including eddies. Thus it is difficult to link changes in those variables to eddy activity alone. SSH, however, is a variable that is closely related to the velocity and scales of eddies and thus is better suited for studies investigating eddy dynamics.

Some of the earliest works based on image processing techniques used an edge detection algorithm to detect eddies along the Gulf Stream (Holyer and Peckinpaugh 1989). Similar image-based algorithms included a neural-network model trained to identify eddies from SST images (Castellani 2006) and an edge detection scheme to isolate eddies between two consecutive SST images (Fernandes and Nascimento 2006). D'Alimonte (2009) used the isothermal lines of the SST field to automatically detect eddies. Finally, Dong et al. (2011) transformed SST observations into a thermal-wind-velocity field and subsequently tracked eddies in the transformed space.

The recent introduction of SSH satellite observations provided researchers with data that are directly related to ocean eddies. The majority of eddy tracking algorithms define eddies as closed contoured (positive or negative) SSH anomalies (see Figure 3). The first of such studies built upon techniques developed previously for turbulence simulations (Isern-Fontanet, García-Ladona, and Font 2003). Since then, numerous variations of the approach used by Isern-Fontanet, García-Ladona, and Font (2003) were introduced, *e.g.* (Fang and Morrow 2003; Chaigneau, Gizolme, and Grados 2008). In the most comprehensive SSH-based eddy tracking study to date, CH11 identified eddies globally as closed contoured smoothed SSH anomalies using a nearest neighbor search.

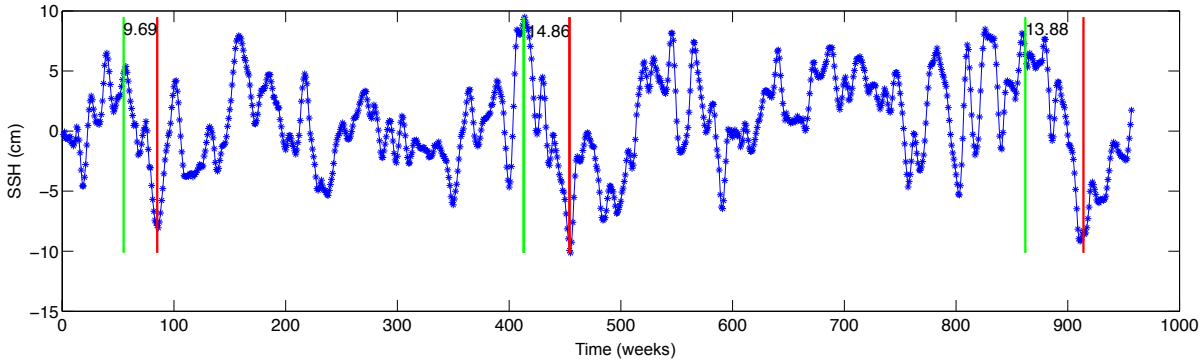

Figure 4: A sample time-series analyzed by PDELTA with gradually decreasing segments enclosed between each pair of green and red lines. These segments were obtained after discarding segments of very short length or insignificant drop that are atypical signatures of an eddy.

They also introduced the notion of eddy non-linearity to differentiate between eddies and Rossby waves. A more detailed review of SSH-based eddy detection methods can be found in Appendix B of CH11.

Despite a large body of work, eddy detection algorithms continue to suffer from several limitations. First, water-surface property signatures such as surface temperature or color do not convey much information on the dynamic process of eddies (Fu et al. 2010). Second, certain SSH-based methods such as those introduced by Chaigneau, Gizolme, and Grados (2008) use derivatives of the SSH field, which amplify the noise in the SSH signal (Chelton, Schlax, and Samelson 2011). Connected component algorithms, such as CH11, tend to be highly parameterized and apply scale-dependent filters to the data to remove features larger (smaller) than a threshold as well as to remove seasonal and internal variability (see Appendix A in CH11 or online supplementary material of (Chelton et al. 2011) for full details on data filtering.) Finally, for each pixel in an SSH snapshot (such as Figure 3), connected component algorithms must search N-nearest neighbors for each pixel making the search space very large as data resolution is increased (see complexity analysis section for details).

3 Methods

Instead of tracking eddies directly in images of SSH anomalies (such as in Figure 3), we propose a novel approach that leverages the fundamental spatio-temporal characteristics of eddies. Eddies form and sustain their energy over a timescale of weeks to months, resulting in gradual changes in SSH on the order of a few centimeters over regions between 50-200 kilometers. Given the large time-scales within which eddies operate, eddies will manifest as a connected group of gradually increasing/decreasing SSH time-series. We leverage this information to track eddies directly from the SSH time-series (see Figure 4) as opposed to the SSH heat-maps.

Our algorithm (adapted from (Chamber et al. 2011)) operates in three main steps, first we identify individual time-series that have the previously described "eddy-like" behavior. Each candidate time-series will be labeled with a start and end time (t_s and t_e respectively) where a significant gradual increase/decrease occurred. Second, given that an eddy must operate over a large enough region, for each time step t we scan the neighbors of any candidate time-series (where $t_s \leq t \leq t_e$); if a sufficient number of neighbors are also candidate time-series at time t then the identified group is labeled as an eddy. Finally, as the eddy moves from one time-step to the next, we keep adding new candidate time-series as their t_s is reached and remove other time-series as their t_e is passed. We count the duration of each eddy as the number of weeks the minimum number of clustered candidate time-series is met.

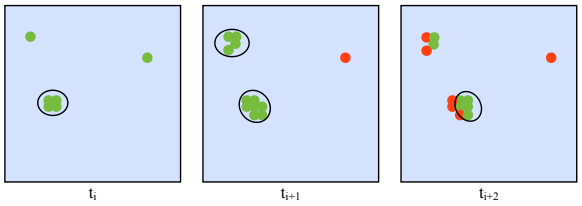

Figure 5: An illustration to show PDELTA's spatial analysis component. At any given time t_i only a subset of all time-series are labeled as candidates for being part of an eddy (green points). Only when a sufficient number of similarly behaving neighbors are detected (in this case four) PDELTA labels them as an eddy (black circle). As time passes, some time-series are removed from the eddy (red points) as they are no longer exhibiting a gradual change; while others are added. If the number of similarly behaving time-series falls below (above) the minimum (maximum) number of required time-series, the cluster is no longer an eddy (*e.g.* top left corner at t_{i+2} frame).

Our approach differs from the original PDELTA described in (Chamber et al. 2011) in two main aspects: first, Chamber et al. (2011) used PDELTA as a time-series change algorithm only. In our case, we augment PDELTA by adding a spatial analysis feature to properly identify clusters of time-series exhibiting similar behavior. Second, the original PDELTA only detected a single increasing (decreasing) segment in a given time-series. In this variation, PDELTA identifies multiple gradually changing segments within a time-series. This is a useful improvement given that an eddy may appear multiple times at the same location. Furthermore, this feature effectively improves our computational performance by mon-

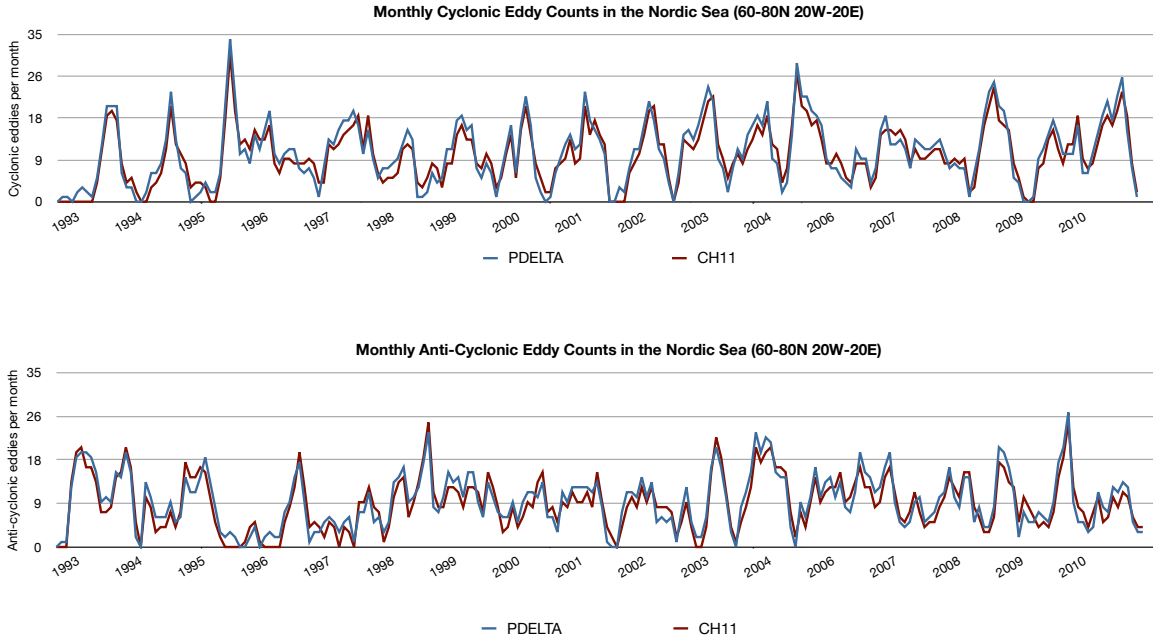

Figure 6: Monthly eddy counts (lifetime $\geq$ 16 weeks). **Top:** Monthly counts for cyclonic eddies as detected by our automated algorithm PDELTA (blue) and CH11 (red). **Bottom:** Monthly counts for anti-cyclonic eddies as detected by our automated algorithm PDELTA (blue) and CH11 (red). Overall, PDELTA detected slightly more eddies than CH11. This could be due to an improved ability to track smaller eddies (see text).

itoring each location (time-series) at most once. For a complete discussion of the original PDELTA algorithm, including experiments, please refer to (Chamber et al. 2011).

Figure 4 demonstrates how our approach detects candidate time-series. The figure shows the SSH anomaly time-series for one grid point in the Nordic Sea. For this particular location, PDELTA identified three segments where a significant gradual decrease in SSH occurred over a long time period starting at approximatively weeks 60, 410, and 870 respectively. During each decreasing segment, we search this location's neighborhood for time-series with similar gradual decrease. Once the significant decreasing segment ends, either there will be other neighbors that will continue to form a coherent eddy or the eddy has dissipated if the minimum eddy size is no longer met (see Figure **??**).

A spatio-temporal approach to eddy detection and monitoring has several advantages: First, we don't apply any filters to our data and have a minimal number of parameters relative to existing approaches. Second, given that we only consider time-series that experience gradual changes in SSH, our algorithm's search space is significantly reduced compared to searching every pixel's neighbors. Finally, since we incorporate a spatio-temporal detection mechanism we can relax some of the minimum/maximum eddy size requirements that space-only connected component algorithms have.

4 Results

We tracked eddies weekly from 1992-2011 in the Nordic Sea region ($60 - 80°$ N and $20°$ W $- 20°$ E) and compared the

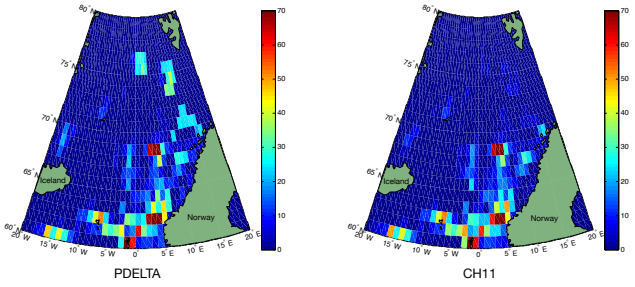

Figure 7: Eddy geographic distribution density. The eddies PDELTA identified (left) were similarly distributed as CH11 (right), except for higher latitudes where PDELTA successfully identified a region known for spawning high latitude eddies (Rossby, Prater, and Søiland 2009) (see Figure 8). Landmasses are colored in dark green.

results with those of CH11[1]. We used the Version 3 dataset of the Archiving, Validation, and Interpretation of Satellite Oceanographic (AVISO) which contains 7-day averages of SSH on a $0.25°$ grid from October 1992 through January 2011.

PDELTA detected slightly more cyclonic (9.89 per month) than anti-cyclonic (9.48 per month) eddies. These differences are consistent with the findings of CH11. Overall, we identified a total of 9.08 eddies per month versus 8.87 for CH11. This could be due to the fact that eddies

[1]Available from: `http://cioss.coas.oregonstate.edu/eddies/nc_data.html`

tend to be smaller in the region analyzed, and thus could have been ignored by CH11's algorithm once the data were filtered. Figure 6 shows the monthly cyclonic (top) and anti-cyclonic (bottom) counts for PDELTA (blue curve) and CH11 (red curve). We find that although the counts match well, PDELTA detected fewer eddies than CH11 during winter months, but more eddies during summer months. This may be due to the gaps in satellite data during winter or simply due to seasonality (*i.e.* fewer eddies in winter time).

To visualize PDELTA's performance compared to CH11, we computed the eddy distribution density based on the locations where eddies were detected. We first divided the Nordic Sea region into 1° cells and counted the total number of eddies passing through each cell. The spatial distribution densities are shown in Figure 7. Both algorithms detect eddies in "active regions" such as near the Norwegian coast. PDELTA, however, finds more eddies than CH11 in higher latitudes possibly because without data filtering we do not wipeout small-scale eddies. The mean radius of eddies decrease approximately monotonically from about 200 km near the equator to about 75 km at 60° latitude (Chelton et al. 2007; Fu et al. 2010), giving our algorithm an advantage to detect such eddies.

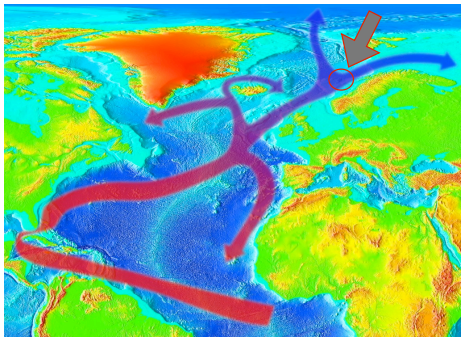

Figure 8: Path of the Gulf Stream (red band) from the tropics to the Arctic. The northern eddies that our PDELTA algorithm identifies in Figure 7 (big gray arrow) is near the region where the Gulf Stream splits generating high latitude eddies that CH11 failed to capture. The existence of such eddies confirmed by field experiments (Rossby, Prater, and Søiland 2009). Figure source: `http://en.wikipedia.org/wiki/Gulf_Stream`

As shown in Figure 8, the northern region captured by PDELTA and not by CH11 (see Figure 7) is where the Gulf Stream splits into the North Cape Current (right split) and the West Spitsbergena (left split) (AMAP 1998). Though different conditions may trigger eddies, they are frequently observed in relation to meandering flows in strong ocean currents (like the Gulf stream (Chelton, Schlax, and Samelson 2011)). Moreover, the region we identified has been specifically monitored using buoyant floats and was found to have noticeable eddy activity (Rossby, Prater, and Søiland 2009). This is further indication that PDELTA is better able to track small eddies.

Although our algorithm has proven capable of monitoring eddies, the increasing size and resolution of climate data make it imperative that algorithms be scalable for large climate datasets. Therefore, for our algorithm to have real world value, it must scale up to the demands of the climate research community.

To test our algorithm's performance on the potential increase in both data resolution and timespan we compared our algorithm's performance to a connected component eddy searching algorithm similar to the one described in Appendix B of CH11. We constructed two datasets from the original data, one where the data's resolution increased up to 100 times (10 times in each grid dimension) and a second where the length of the time-series increased up to 100 times. We then tracked eddies at weekly intervals for the entire period covered by the data.

Computational Complexity. For a grid with $M \times N$ observations and time-series length K, the time complexity of PDELTA is linear in the number of grid cells, and the time-series length (*i.e.* $O(MNK)$). On the other hand, connected component algorithms are quadratic in the number of grid cells, (*i.e.* $O((MN)^2K)$). The space requirements of both approaches are modest. Figure 9 shows empirical results comparing the computation time of PDELTA and the connected component algorithm as the number of grid cells ($M \times N$) and time-series length (K) are increased; the figure shows quadratic increase in computation time for the connected component algorithm as $M \times N$ is increased, while PDELTA's computation time increases linearly. This difference is particularly germane since data from future climate models and satellite observations will be of much higher resolution ($M \times N$ is expected to increase by orders of magnitude) than today's datasets and will approach 100s of petabytes (Overpeck et al. 2011).

5 Discussion & Future Work

We presented an automated, accurate, and scalable eddy detection and monitoring algorithm based on gradual changes in SSH time-series. While unique, our approach currently suffers from several limitations: First, our minimum and maximum eddy size criteria are hard-coded parameters. Given that we do not filter our data, large-scale phenomena such as gyres and currents are still present in the data and can be mistaken for very large eddies. Conversely, although we are able to detect smaller eddies than CH11, we must ensure that a sufficient number of neighboring time-series experience similar gradual change. To address this issue we imposed a user-specified minimum and maximum eddy size. Future iterations of the algorithm would benefit from automatic parameter estimation that adapts minimum and maximum eddy size based on latitude, since eddy sizes vary as a function of latitude (Fu et al. 2010). Another potential investigation could be a sensitivity study of our algorithm's performance to the space and time thresholds mentioned above.

Second, our algorithm does not account for gaps in the data and simply ignores missing values. That is why certain weeks will have very low eddy counts, especially during winter, when precipitation obstructs satellite visibility. Previous works have addressed this challenge by using extrapolation to fill in missing data (Chelton et al. 2011). Although

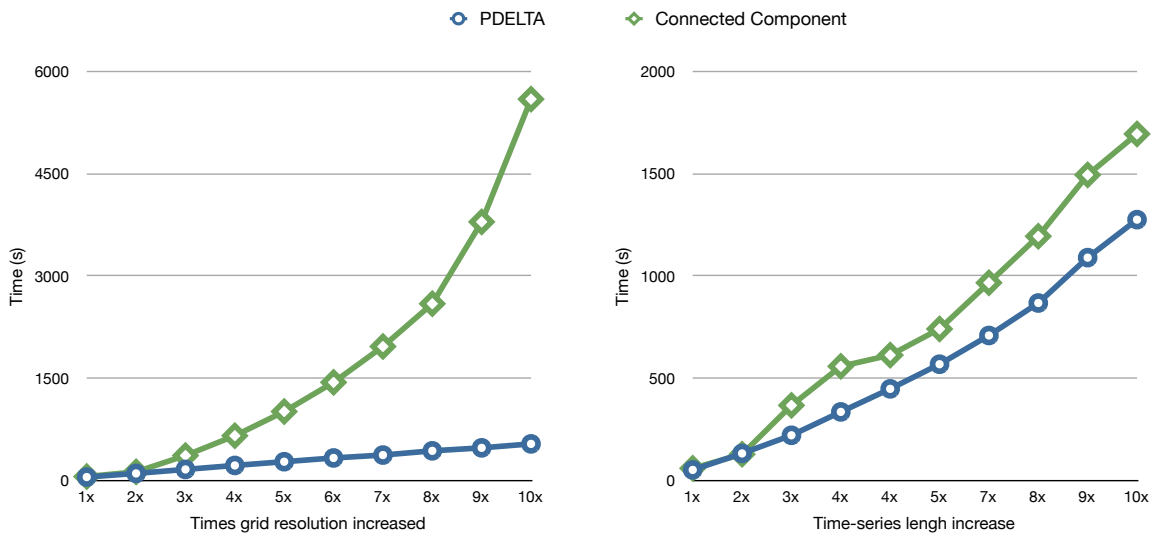

Figure 9: Scalability comparison between our algorithm PDELTA (blue) and a connected component algorithm (green) similar to CH11. **Left:** time required to track all eddies in the dataset as a function of the grid resolution. **Right:** time required to track all eddies in the dataset as a function of the time-series length (*i.e.* number of weekly observations). Our algorithm PDELTA (blue) scales better than the connected component algorithm in both time and space.

our algorithm can take advantage of extrapolation, such an approach is not ideal since the factors that impact most climate data such as SSH are highly non-linear, whereas existing extrapolation techniques are not and, therefore, cannot capture such influences. Such a limitation significantly decreases the reliability of data extrapolation. Instead, we would propose to use time-series interpolation algorithms, which have recently been studied in the context of seasonal earth science data (Hird and McDermid 2009) as well as established matrix completion techniques (Candès and Recht 2009).

Third, previous studies investigating eddy dynamics have mistaken eddies with Rossby waves (large-scale ocean variability that masquerades as an eddy). Because we analyze global data, and given that we do not filter the data beforehand, there is an increased likelihood of false-positives. To address this issue, CH11 used the eddies' nonlinearity (the ratio of an eddy's rotational and transitional speeds) as a mechanism to differentiate between eddies and Rossby waves. In future work, we will add this type of discriminant to eliminate Rossby waves from our analysis. It is important to note that this issue does not impact our current analysis given that Rossby waves are easily discernible from ocean eddies at high latitudes (Fu et al. 2010).

Finally, although we report similar monthly eddy counts and spatial distribution as CH11, we must caution that analyzing eddy count alone is an incomplete comparison to CH11. Additional eddy statistics and kinematic properties such as eddy size and speed must be analyzed to fully compare PDELTA to CH11.

Despite these limitations, our algorithm produces similar counts to the state-of-the-art eddy tracking algorithms by leveraging the natural spatio-temporal characteristics of eddies. Additionally, it is capable of identifying regions that other algorithms cannot and these regions have been corroborated by field studies (Rossby, Prater, and Søiland 2009). Identifying small eddies (< 100km) has been challenging for connected component techniques given current data resolution and filtering techniques. By monitoring SSH patterns through changes in the time-series as opposed to visual images, we are able to capture smaller eddies than possible with the existing approaches. Finally, as opposed to common connected component algorithms that run quadratically in the grid resolution, PDELTA runs in linear time – a significant improvement given the expected dramatic increase in climate data (Overpeck et al. 2011).

We foresee our algorithm being used in other domains where one is interested in automatically monitoring gradual changes in time-series data. A recent paper by Giles et al. (2012) monitored the western Arctic Beaufort Gyre using SSH from satellite data. Automatic gyre monitoring can also be an application to our algorithm. While this line of research is critical to understanding future ocean dynamics and marine ecosystems, it also has important applications to time-series and matrix completion, scalable learning algorithms, and spatio-temporal data mining.

6 Acknowledgments

This work was funded by an NSF Graduate Research Fellowship, an NSF Nordic Research Opportunity Grant, the Norwegian National Research Council, the Planetary Skin Institute, NSF Grant IIS-0905581, and an NSF Expeditions in Computing Grant (#1029711). The authors are grateful to Dudley Chelton for helpful comments that improved the clarity of the manuscript. Access to computing resources was provided by the University of Minnesota Supercomputing Institute.

7 Appendix

The pseudo-code for PDELTA is listed in Algorithm 1. α and β are the start and end time steps for a decreasing segment, and subscript j tracks the number of such segments. Ł is the loss (or gain) in height due to the decrease (increase).

Algorithm 1 PDELTA algorithm for gradual decrease detection.

$n =$ number of time steps in the time-series T
$S =$ season length
$v = v_1, v_2, ..., v_n$ (time-series values)
for $t = S \rightarrow n - S$ **do**
  $\Delta_t \leftarrow mean(v_{t-S+1} \cdots v_t) - mean(v_{t+1} \cdots v_{t+S})$
end for
$j \leftarrow 0$
$t \leftarrow S$
while $t \leq n - S$ **do**
  if $\Delta_t > 0$ **then**
    $j \leftarrow j + 1$
    $\alpha_j \leftarrow t$
    while $\Delta_t > 0$ **do**
      $t \leftarrow t + 1$
    end while
    $\beta_j \leftarrow t$
    $Ł_j \leftarrow \frac{\sum_{t=\alpha_j}^{\beta_j} \Delta_t}{S}$
  end if
  $t \leftarrow t + 1$
end while

References

AMAP, A. 1998. assessment report: Arctic pollution issues. *Arctic Monitoring and Assessment Programme (AMAP), Oslo, Norway* 12:859.

Candès, E., and Recht, B. 2009. Exact matrix completion via convex optimization. *Foundations of Computational Mathematics* 9(6):717–772.

Castellani, M. 2006. Identification of eddies from sea surface temperature maps with neural networks. *International journal of remote sensing* 27(8):1601–1618.

Chaigneau, A.; Gizolme, A.; and Grados, C. 2008. Mesoscale eddies off peru in altimeter records: Identification algorithms and eddy spatio-temporal patterns. *Progress in Oceanography* 79(2-4):106–119.

Chamber, Y.; Garg, A.; Mithal, V.; Brugere, I.; Lau, M.; Krishna, V.; Boriah, S.; Steinbach, M.; Kumar, V.; Potter, C.; and Klooster, S. A. 2011. A novel time series based approach to detect gradual vegetation changes in forests. In *CIDU 2011: Proceedings of the NASA Conference on Intelligent Data Understanding*, 248–262.

Chelton, D.; Schlax, M.; Samelson, R.; and de Szoeke, R. 2007. Global observations of large oceanic eddies. *Geophysical Research Letters* 34:L15606.

Chelton, D.; Gaube, P.; Schlax, M.; Early, J.; and Samelson, R. 2011. The influence of nonlinear mesoscale eddies on near-surface oceanic chlorophyll. *Science* 334(6054):328–332.

Chelton, D.; Schlax, M.; and Samelson, R. 2011. Global observations of nonlinear mesoscale eddies. *Progress in Oceanography*.

D'Alimonte, D. 2009. Detection of mesoscale eddy-related structures through iso-sst patterns. *Geoscience and Remote Sensing Letters, IEEE* 6(2):189–193.

Denman, K., and Gargett, A. 1983. Time and space scales of vertical mixing and advection of phytoplankton in the upper ocean. *Limnology and Oceanography* 801–815.

Dong, C.; Nencioli, F.; Liu, Y.; and McWilliams, J. 2011. An automated approach to detect oceanic eddies from satellite remotely sensed sea surface temperature data. *Geoscience and Remote Sensing Letters, IEEE* (99):1–5.

Fang, F., and Morrow, R. 2003. Evolution, movement and decay of warm-core leeuwin current eddies. *Deep Sea Research Part II: Topical Studies in Oceanography* 50(12-13):2245–2261.

Fernandes, A., and Nascimento, S. 2006. Automatic water eddy detection in sst maps using random ellipse fitting and vectorial fields for image segmentation. In *Discovery Science*, 77–88. Springer.

Fu, L.; Chelton, D.; Le Traon, P.; and Morrow, R. 2010. Eddy dynamics from satellite altimetry. *Oceanography* 23(4):14–25.

Giles, K. A.; Laxon, S. W.; Ridout, A. L.; Wingham, D. J.; and Bacon, S. 2012. Western arctic ocean freshwater storage increased by wind-driven spin-up of the beaufort gyre. *Nature Geosci* advance online publication:–.

Gnanadesikan, A.; Emanuel, K.; Vecchi, G.; Anderson, W.; Hallberg, R.; et al. 2010. How ocean color can steer pacific tropical cyclones. *Geophysical Research Letters*.

Hansen, C.; Kvaleberg, E.; and Samuelsen, A. 2010. Anticyclonic eddies in the norwegian sea; their generation, evolution and impact on primary production. *Deep Sea Research Part I: Oceanographic Research Papers* 57(9):1079–1091.

Hird, J., and McDermid, G. 2009. Noise reduction of ndvi time-series: An empirical comparison of selected techniques. *Remote Sensing of Environment* 113(1):248 – 258.

Holyer, R., and Peckinpaugh, S. 1989. Edge detection applied to satellite imagery of the oceans. *Geoscience and Remote Sensing, IEEE Transactions on* 27(1):46–56.

Isern-Fontanet, J.; García-Ladona, E.; and Font, J. 2003. Identification of marine eddies from altimetric maps. *Journal of Atmospheric and Oceanic Technology* 20(5):772–778.

Overpeck, J.; Meehl, G.; Bony, S.; and Easterling, D. 2011. Climate data challenges in the 21st century. *Science* 331(6018):700.

Rossby, T.; Prater, M.; and Søiland, H. 2009. Pathways of inflow and dispersion of warm waters in the nordic seas. *Journal of Geophysical Research* 114(C4):C04011.